Hot-Wire Calorimeter Study of Ion Production and Acceleration

V A Sandborn* and L V Baldwin*
Colorado State University, Fort Collins, Colo

Detailed performance characteristics are presented for a porous tungsten ion source with an electrostatic Pierce accelerator system This system is similar in principle to proposed space propulsion systems Cesium ion production was accurately predicted from free molecular flow calibrations of the porous tungsten ionizer Measured critical emitter temperatures exhibited a hysteresis which was explained by Taylor and Langmuir's data for cesium contact ionization on solid tungsten Hot-wire calorimeter surveys of the beam were used to evaluate the performance of a cylindrical Pierce accelerator system employing a virtual or plasma-potential "decelerator " The loss of performance due to the exit electrode aperture was compared with theory for accelerator aspect ratios ranging from 0 6 to 1 3 The total beam power available from a given accelerator geometry (Child's law) was greatly increased by a countercurrent electron flow which issued from a local electron emitter placed within the accelerator This countercurrent electron configuration may offer a means of obtaining large improvements in engine efficiency

Nomenclature

D = ion emitter diameter, m
J = ion beam current, amp
j = ion beam current density, amp/m^2
L = physical dimension from ion emitter to Pierce accelerator, m
ΔP = pressure difference across porous tungsten emitter, mm Hg
T = ion emitter temperature, °R
T' = cesium vaporizer temperature, °R
V = potential, v
ΔV = accelerating voltage (potential difference between ion emitter and accelerator, v)

Introduction

ELECTROSTATICALLY accelerated ions may serve in the future as a useful space propulsion system [1 2] Research and development programs are underway to develop practical ion rocket systems Several new diagnostic techniques have been developed to assist in the experimental evaluation of ion thrustors The hot-wire calorimeter is one of these new research tools [3 4] This resistance temperature transducer measures the ion beam-power density at a point, and surveys of the probe may be used to obtain the power distribution throughout the beam Hot-wire calorimeters have been used in the work reported here to study the production of cesium ions by contact ionization on porous tungsten and to evaluate an analytically designed electrostatic accelerator

The ion source and accelerator system employed herein is not proposed as a practical space propulsion system Rather, the device is considered as a research tool, both to develop diagnostic techniques and to study the basic physics of ion beams This article is a detailed study of some of the physical processes of a porous tungsten emitter of cesium ions and a cylinderical Pierce accelerator Several important design criteria were experimentally checked, and some unexpected but potentially important phenomena were discovered in the course of the research

Received by IAS June 15, 1962; revision received January 27, 1964 The research reported in this paper was done while the authors were employed at the NASA Lewis Research Center, Cleveland, Ohio

* Associate Professor Member AIAA

Apparatus and Procedure

Vacuum Facility

The experiments were conducted at a side port of one of the approximately 5 × 19 ft, high-vacuum tanks used for electric thrustor research at NASA Lewis Research Center [5] The pressure within the tank was maintained between 10^{-7} and 10^{-6} torr for all tests, but the bell jar that housed the ion apparatus was normally operated at an order of magnitude higher pressure

A viewing port was located across the tank from the bell jar The porous tungsten emitter could be viewed through this port with an optical pyrometer The window became coated during the tests, resulting in indicated emitter temperatures that may be as much as 100°F too low However, for the data reported on critical emitter temperatures, this source of error was eliminated by a direct calibration through the window

Ion Source

Figure 1 is a sketch of the ion source and accelerator, drawn dismantled for ease of viewing A commercial porous tungsten emitter was chosen to obtain a relatively uniform distribution of ions for the accelerator study A porous tungsten disk (0 048 in thick) was brazed into a molybdenum tube having a 1-in i d The braze filled the edges so that the effective radius for ion emission was found, by a wetting technique, to be 0 82 in The molybdenum tube was mounted with a stainless-steel "O" ring seal to a copper chamber called the vaporizer A radiant heater, not shown in Fig 1, was inserted around the molybdenum tube The molybdenum-tube conduction heats the porous tungsten to any desired temperature The conduction through the "O" ring is sufficient, also, to overheat the vaporizer, and so air-cooling tubes were wrapped around the chamber for temperature control

The temperature of the vaporizer determines the amount of cesium vapor that flows through the emitter Normal operation required the emitter to be heated to around 2000°F, while the vaporizer was held below 300°F with cooling air When a thermal steady state was attained, a glass capsule containing cesium metal was broken within the vaporizer by a plunger Some cesium was vaporized and flowed through the porous tungsten disk Cesium molecules were ionized by the hot

tungsten surface; the ions were accelerated from the emitter surface by the electrostatic accelerator system

Accelerator System

The tungsten emitter is operated at a positive potential, thereby accelerating the singly charged, positive cesium ions For the test reported here, the emitter, molybdenum tube, emitter heater, and vaporizer were all maintained between 1 and 10 kv, positive with respect to ground A beam-forming electrode, shown in Fig 1, was mounted in physical contact with the tungsten emitter to control the initial focus of the beam This cone-shaped electrode forced the ion trajector to be nearly perpendicular to the emitter despite the beam space charge The focusing electrode had an aperture 0 82 in in diameter to match the emitter

The accelerator electrode was supported parallel to the focusing electrode and operated between 1 to 10 kv potential negative with respect to ground The accelerator aperture was 1 in in diameter As noted earlier, no final or grounded electrode was employed Two accelerator assembles, other than the Pierce design, were also used in this research

In the design of the Pierce accelerator, a uniform current density was assumed to flow normally and one dimensionally from the emitter in a space-charged limited beam This saturation current density was calculated from Child's solution of Poisson's equation,

$$j = 4\,75 \times 10^{-9} (\Delta V^{3/2}/L^2) \qquad (1)$$

where the constant corresponds to singly charged cesium ions The electrode design, to obtain these conditions in a cylindrical beam, was calculated from Daykin's series solution of Laplace's equation with the Pierce boundary conditions [6] The beam-focusing electrode, which rests on the ion emitter surface, makes an angle of 67 5°, with the emitter as prescribed by Pierce (Ref 7, p 181) The single accelerating electrode had an approximate 22° initial angle A more detailed discussion of the accelerator design method may be found in Ref 8

Two other accelerating electrodes were used in the tests The Pierce electrode had a vertical set of tantalum grid wires, spot welded on 0 08-in centers extending across the aperture to evaluate the effect of the exit hole For the critical emitter temperature tests, the beam-forming electrode was removed, and a simple, straight grid-wire assembly was substituted for the Pierce accelerating electrode This grid accelerator suffered from severe sputtering damage and ultimate failure, but the closer spacing increased the beam current density

A thoriated tungsten electron emitter, shown in Fig 1 as an 0 57-in -diam ring, was attached by insulators to the beam-forming electrode This electron emitter and its power supply were present in only one set of experiments, which are described in the section entitled "a possible improvement of the thrustor "

Instrumentation

As shown in the electrical schematic in Fig 1, the important beam currents and accelerating potentials were monitored by meters The vaporizer temperature was measured by thermocouples A disappearing filament-type of optical pyrometer was used to measure the ion emitter temperature A small temperature gradient of 20–50°F existed across the emitter due to the form of conduction heating used, but only an average emitter temperature was recorded

A single hot-wire calorimeter probe was used to measure the power distribution throughout the ion beam Similar probes are described in Ref 3; a 0 0004-in -diam platinum-iridium wire, 0 20 in long, was employed for all measurements The probe traversed the beam at an axial position 7 1 in downstream of, and parallel to, the plane of the emitter The probe passed across the beam diameter

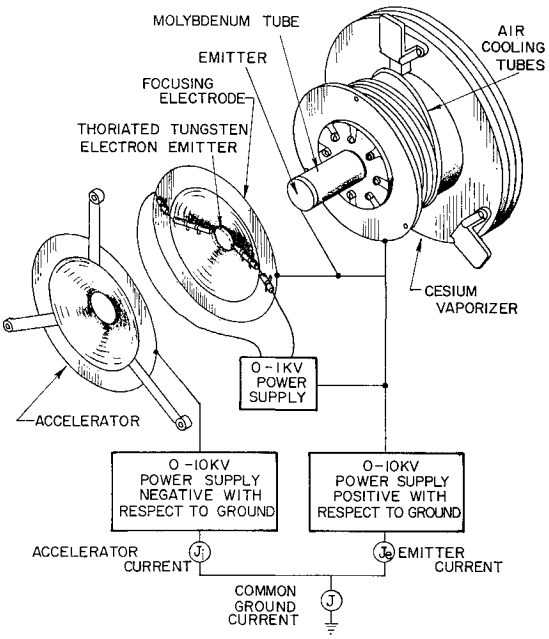

Fig 1 The ion thrustor

Test Results and Discussion

Ion Beam Measurements

In an initial experiment, the cylindrical symmetry of the beam was directly observed from sputtering patterns on a copper plate calorimeter described in Ref 9 In all future research, the hot-wire calorimeter surveys across the beam radius were weighted appropriately to calculate the total beam power in a digital computer program Typical hot-wire surveys are shown in Fig 2 The upward shift of the dotted base line of each profile is due to a slight increase in probe support temperature and the thermal radiation from the ion emitter This zero drift can be theoretically calculated as demonstrated in Ref 4; the local beam power is proportional to the vertical distance between the solid and dashed curves

Figure 3 compares a typical set of total power measurements calculated from current and voltage meters The net current to ground J times the voltage on the ion emitter should equal the total power in the beam, if no external electrons from the

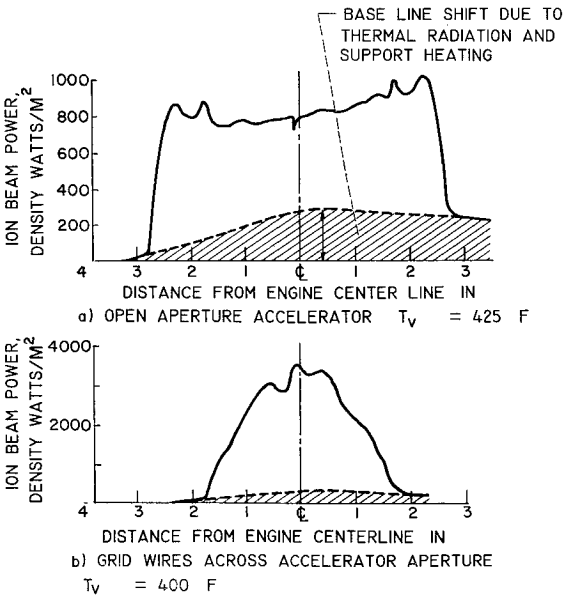

Fig 2 Typical hot-wire calorimeter traces, L/D = 0 87, emitter at +5 kv, accelerator at −2 kv

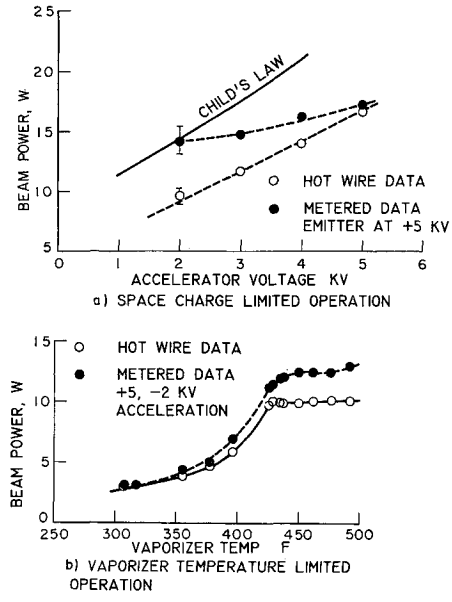

Fig 3 Effect of external electrons on metered beam power, $L/D = 0.87$

test facility backstream into the emitter The regions of data disagreement in Fig 3 are systematic in a manner that implies extraneous electrons have entered from the plasma of the vacuum facility into the electrical circuit Figure 3a shows that the meter and calorimeter measurements systematically approach agreement as the accelerator voltage is increased As will be shown later, aperture effects cause the actual beam power to be less than Child's law The meter values in Fig 3a are high, particularly at small negative accelerator potentials Extraneous electrons are effectively "cut off" at the larger, negative potentials Figure 3b shows the effect of vaporizer temperature, which is a measure of ion beam density below space-charge limited operation The denser the beam of positive ions, the more likely extraneous electrons will be able to penetrate to the emitter

Under favorable conditions, the meters and the hot-wire measurements agree; disagreement that does occur appears systematic in the metered power data Therefore, the hot-wire results are assumed to be correct for all operating conditions in the remainder of the report Meter currents are reported only in Figs 4–6, which are concerned with the critical ionizer current density data and accelerator impingement data

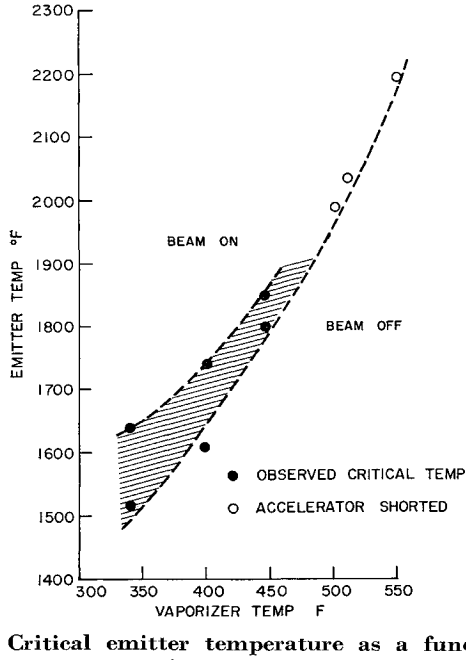

Fig 4 Critical emitter temperature as a function of vaporizer temperature

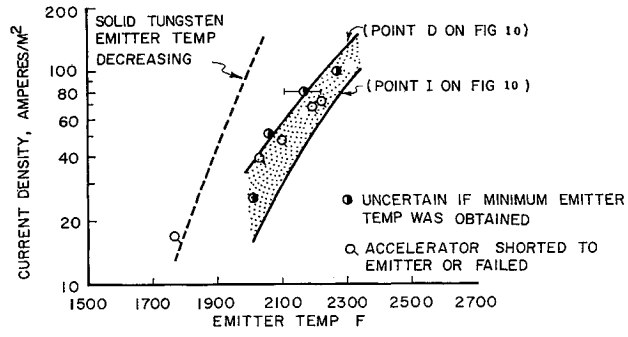

Fig 5 Comparison of observed maximum current density at different emitter temperatures with analysis of Reynolds [10] All data for 5-μ-diam pore, porous tungsten emitter The emitter temperature was being decreased in all cases

Ionizer Study

Ion source calibration

The porous tungsten characteristics were evaluated from gaseous nitrogen flow rate measurements As shown in Ref 10, the volumetric flow rate vs pressure drop data can be used to calculate the average pore size of the tungsten emitter Figure 7 is the gas flow calibration obtained for the present emitters; using the procedures of Ref 10, an average pore diameter of 5μ was inferred from these data In operation, the vapor pressure of cesium in the vaporizer is maintained between 5×10^{-4} and 1 mm Hg Although 1 mm Hg is the lower limit of the gas calibration rig (Fig 7), the flow below $\Delta P = 10$ mm Hg is free molecular for these samples; note the direct proportionality of flow rate to ΔP in this region The nitrogen flow rate at 1 mm Hg was converted into an equivalent cesium ion current:

$$J = 3.11 \times 10^{-2}\, \Delta P\, (492/T)^{1/2} \qquad (2)$$

Figure 8 is a plot of Eq (2) prepared from the cesium vapor

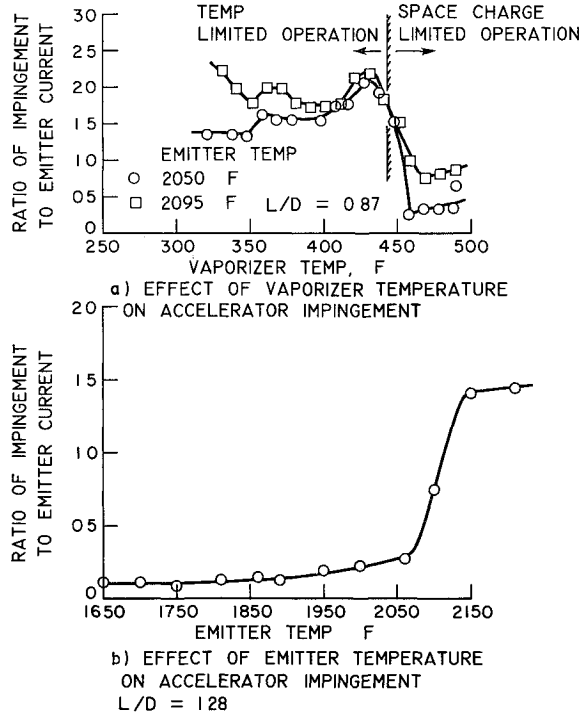

Fig 6 Accelerator impingement characteristics

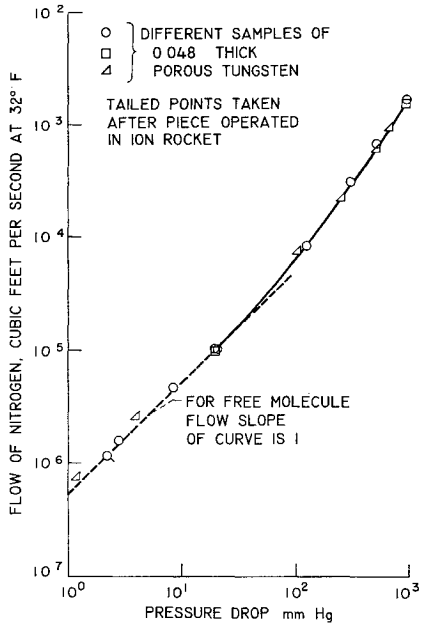

Fig 7 Cold flow calibration of the porous tungsten emitters

pressure ΔP vs vaporizer temperature T of Ref 11 The data shown in Fig 8 for actual ion beam operation were obtained with the grid-wire accelerator These data show that the assumption of unit ionization efficiency, which was used to calculate Eq (2), is at least approximately valid The discrepancy between theory and observation at low current densities is traceable to residual ions, which were always found with the emitter hot That is, even though the porous tungsten was chemically cleaned after each test, an ion beam was observed *before* a new cesium capsule was broken This beam has an unknown composition and it determines the "noise level" of the experiment Unfortunately, it was impractical to allow the ionizer to clean in operation before each test

The ionizer temperature should have a great effect on the efficiency of cesium ionization Figure 9 shows an example of this effect as a plot of total beam power measured well within the "vaporizer limited" range of operation That is, the grid-

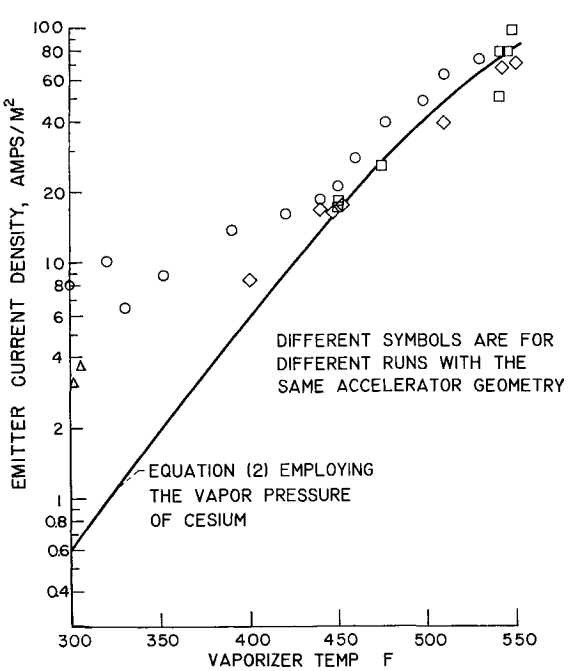

Fig 8 Predicted and experimental emitter current as a function of vaporizer temperature

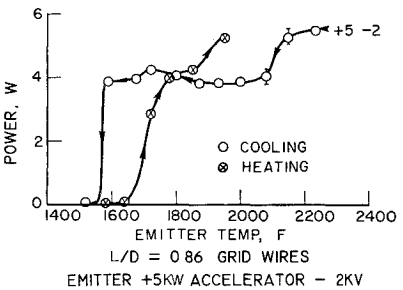

Fig 9 Beam-power variation with emitter temperature

wire Pierce accelerator has a space-charge flow limitation well above the beam observed in Fig 9, so that the limit observed in beam power is governed by the rate of neutral cesium flow through the tungsten In the example shown in Fig 9, the arrival rate of neutral cesium was maintained at a constant value, and only the emitter temperature was varied At some "critical temperature" the production of ions greatly diminished when the emitter was cooled Heating the emitter resulted in a different, higher critical temperature This hysteresis can be explained from the classical study of cesium contact ionization on tungsten by Taylor and Langmuir [12] Although their experiments were performed on solid tungsten, the qualitative results are similar to those reported here

Reynolds and Childs[13] have replotted the evaporation data in terms of total evaporation rates (ions plus atoms) as a function of monolayer absorbed on the tungsten Following the work of Reynolds and Childs, a curve of fraction of monolayer absorbed on the surface against the tungsten emitter temperature at a constant arrival rate may be constructed as shown in Fig 10 Now consider what happens as the emitter temperature is decreased from point D to E, the only point on the curve corresponding mainly to atoms and not ions; thus, the ion beam is reduced to a very low value If the emitter temperature is now increased from E to F, the layer absorbed decreases along the atom curve As the temperature increases from points F to G to H, the ion beam begins to reappear, as some ions as well as atoms are evaporated from the tungsten surface Upon reaching an emitter temperature at point I, the fraction of a monolayer absorbed decreases sharply to the ion curve, and the production of ions is greatly increased

Figure 4 shows the measurements obtained for the critical emitter temperature against neutral cesium flow rate (vaporizer temperature) for the present emitter The open points shown on Fig 4 were obtained with the straight grid-wire accelerator, whereas the solid points were taken with the Pierce

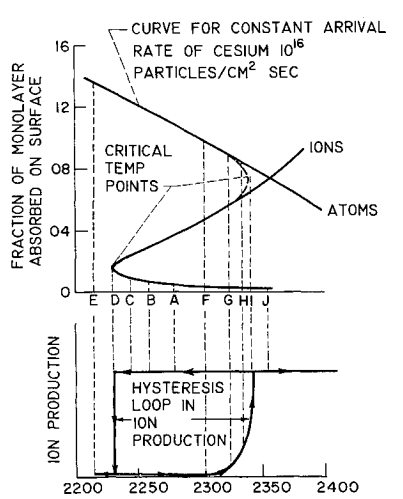

Fig 10 Ion production hysteresis loop predicted from Taylor and Langmuir's data on the evaporation of cesium from tungsten

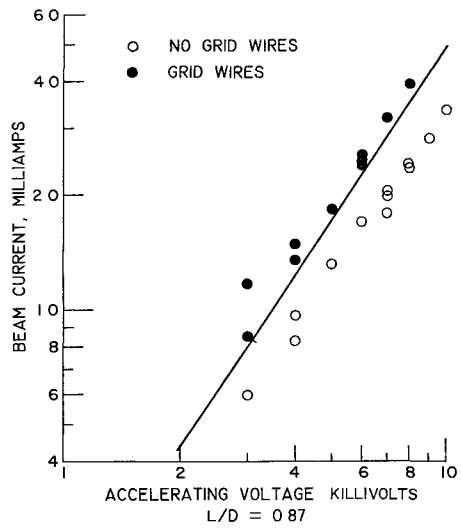

Fig 11 Comparison of measured space-charge beam current with Child's law

accelerators In all cases, with the straight grid wires, no true beam shutoff was observed Rather, a point was reached where the negative accelerator appeared to short-out directly to the positive emitter In each case the apparent short disappeared when the operating conditions (e g , T or T) were changed from the near critical conditions, which suggests that neutral cesium vapor may have caused an electrical coupling in the short accelerator region The lower curve in Fig 4 corresponds to the point D of Fig 10 because it was obtained by lowering the emitter temperature The upper curve corresponds to point I; these data were measured by increasing the emitter temperature Although the beam on-off and hysteresis phenomena observed on porous tungsten have a qualitative counterpart on solid tungsten, the porous tungsten transitions seem more gradual than the data of Taylor and Langmuir This might be attributed to uneven distribution of ion emitting areas, as the ion microscope movies of Electro-Optical Systems suggest [14]

Reynolds[10] has evaluated the maximum current density for porous tungsten at the critical emitter temperature, using the data of Taylor and Langmuir Reynold's predictions for a 5-μ-pore diameter emitter are shown in Fig 5 Figure 5 includes data taken with the grid-wire accelerator assembly near the critical emitter temperature (point D on Fig 10) Although definite conclusions cannot be drawn because of insufficient data, Fig 5 shows that the predictions of Ref 10 may be reliable

Pierce Accelerator Characteristics

Total beam power

The present accelerator system was chosen because analytical solutions for electrode design were readily available [7] However, the analytical design neglects the beam-exit hole in the accelerator, so that the potential field of the analysis is in error for any real design It is easy to see on a membrane analog that the effect of this exit aperture is to bow the electrode

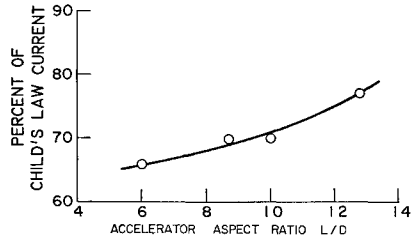

Fig 12 Summary of aperture effect on beam current

equipotential surface in toward the emitter This defocusing effect is accentuated for small ratios of accelerator length L to beam diameter D (L/D = aspect ratio) Since short accelerator lengths are essential for reasonable engine efficiency [e g , see Eq (1) for j], one of the experimental objectives was to test the deviation from Child's law due to the aperture effect

Figure 11 shows an example of space-charged limited current for a fixed spacing of the Pierce accelerator The beam current J was calculated from hot-wire calorimeter beam-power integrations:

$$J = \frac{\text{total beam power}}{\text{emitter potential}}$$

The acceleration voltage shown in Fig 11 is the voltage difference between emitter and accelerator A $\frac{3}{2}$ power law line through the open data points was used to determine the loss in theoretical performance traceable to the exit aperture at an L/D = 0 87 A summary plot of the derivation from Child's law as a function of accelerator aspect ratio is given in Fig 12 As might be expected, the deviation is reduced by increasing the accelerator L/D, though this improvement results in a severe loss of total beam power

Grid wires placed across the Pierce accelerator would be expected to reduce the bowing of the accelerator equipotential Figure 11 shows that data obtained with such an accelerator are in close accord with Child's law predictions The practical problem, of course, is the severe sputtering damage incurred on the grid wires

Beam spreading

The width of the ion beam was measured by the hot-wire calorimeter at a station 7 1 in downstream of the emitter Space does not permit a detailed presentation of these results, but a brief summary may be useful With the ordinary Pierce accelerator and virtual decelerator, the beam spreading could be attributed to a combination of space charge and lens action for $\Delta V/V < 2$ At large accelerating voltage ΔV, the ob-

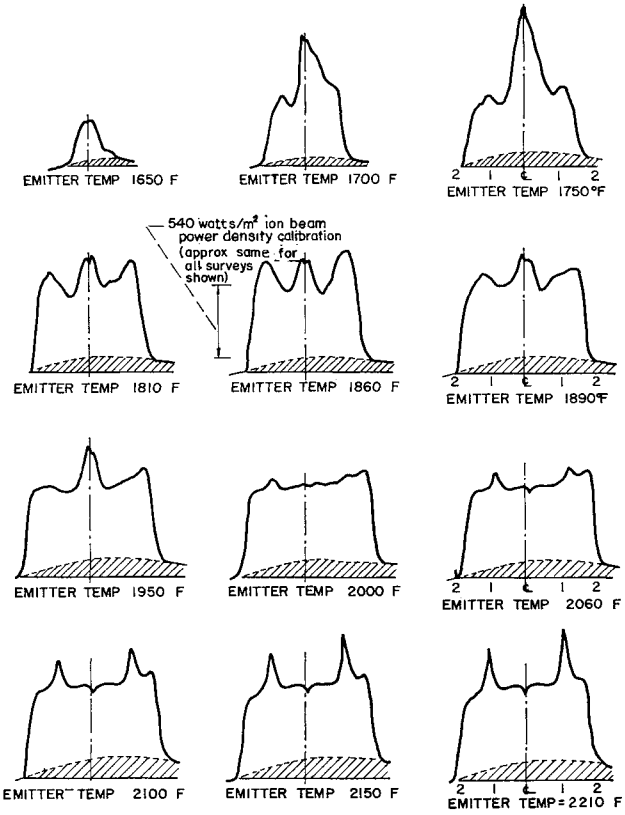

Fig 13 Effect of accelerator impingement on the beam-power distribution, L/D = 1 28

served spreading was much less than that predicted by space-charge theory alone With the Pierce accelerator with grid-wire aperture, the beam spreading observed could be accounted for by paraxial space change flow estimates

Accelerator impingement

A practical ion rocket will require negligible impingment of ions on the accelerator For this reason, analytical and analog design techniques have been perfected [15] On the other hand, real ion thrustors may operate off-design (i e , at other than space-charge limited currents) and the present study has yielded several interesting observations concerning accelerator impingement over a wide range of conditions

Some impingement and sputtering was encountered on the accelerator in all of the tests reported With accurate electrode alignment, the impingement followed a trend indicated in Fig 6a The sharp minimum in percent impingement occurs at approximately the design point of space-charge limited flow The minimum is bounded by an increase in accelerator impingement for less than space-charge limited flow, and a more gradual increase at the higher neutral cesium flow rates The region of vaporizer temperatures just below the minimum was observed to be a highly unstable operating condition for the system

In Fig 6a, the accelerator impingement appears to be systematically higher in the space-charge limited region when the emitter temperature is increased Figure 6b confirms this effect, which is probably caused by the increased thermal velocity of the emitted ions A striking change in the beam-power distribution was observed as the impingement rose on accelerator It might be argued that the increased thermal velocities of the emitted ions resulting from the high emitter temperatures should cause a noticeable effect on the over-all

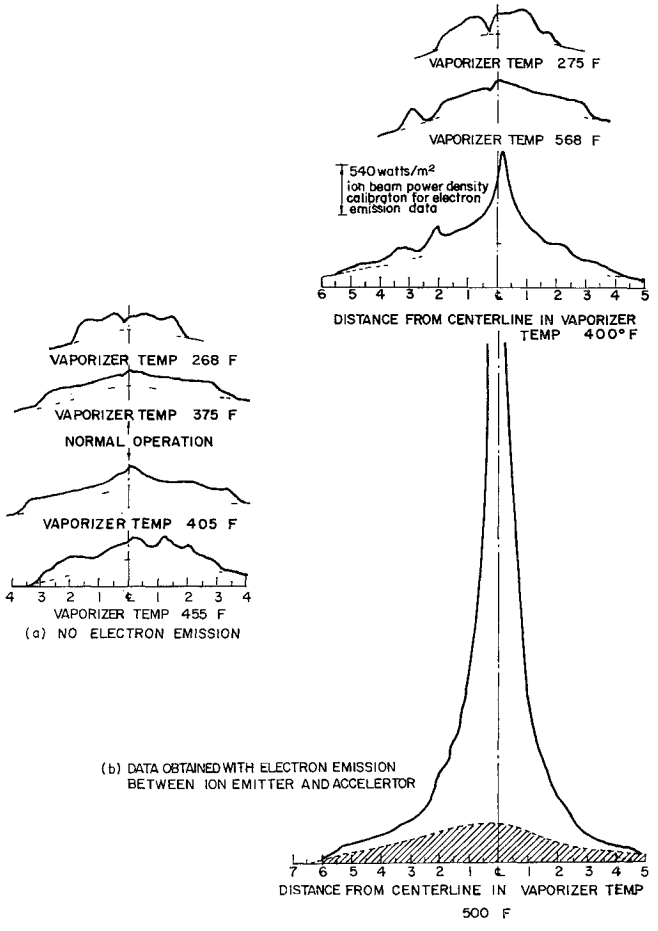

Fig 14 Increase in beam power available due to the electron emitter-accelerator system, $L/D = 1\,0$

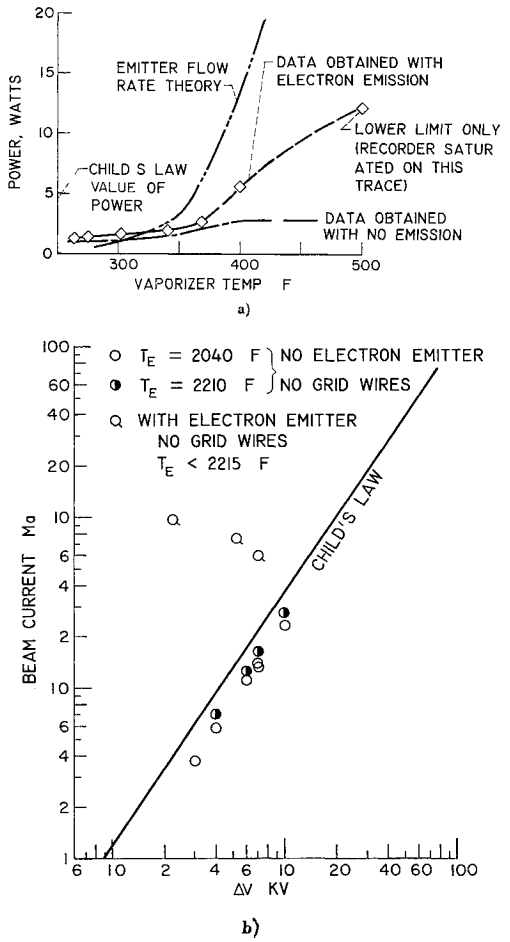

Fig 15 a) Vaporizer temperature effect—comparison of the electron emitter-accelerator system with normal operation (emitter voltage + 2 kv, accelerator voltage −5 kv) b) Accelerating voltage effect—concluded Comparison of the output of the electron emitter-accelerator system with normal operation, $L/D = 1\,0$

beam shape However, what was actually observed (Fig 13) were local maximums in the power density near the edge of the beam The small power increase calculated from these profiles with local maximums correlated well with an observed increase in metered current J The authors speculated that the local beam-power increases were due to secondary electrons, which were created by the impingement, backstreaming into the emitter Perhaps these very fast secondary electrons create a local cloud of slow secondary electrons when they strike the ion emitter This cloud of retarded secondary electrons might reduce the local positive space charge in the region near the ion emitter surface

Further evidence that the calorimeter was actually indicating local peaks in the ion beam was supplied by the sputtering pattern on the Pierce grid-wire accelerator A circular ring of intense sputtering occurred at the wires on a diameter, which was smaller than the exit aperture and which appeared to correspond to the power peak shown in Fig 13 It seems unlikely that electrons could strike the grid wires because of their high negative potential The straight grid-wire accelerator, unlike the Pierce electrode, did not have a solid outer surface, and no local increases in the ion beam power were observed Therefore, all experimental evidence supports the hypothesis that ion accelerator impingement is tied directly to local increases in ion beam power

A possible improvement of the thrustor

The unexpected results just described led to a possible improvement in electrostatic thrustor design For these tests, a

controllable electron emitter was mounted in a 0 52-in ring on the focusing electrode by insulators as shown in Fig 1 The emitting wire circle was positioned about 0 15 in above the ion emitter, so it was well within the 0 82-in accelerator length employed ($L/D = 1\ 0$) In operation, the potential of the electron emitting ring was set near the local space-charge potential in the ion beam; this potential was usually within a few hundred volts of the positive ion emitter The externally heated electron ring boiled off electrons that fell into the ion emitter because of the high negative potential of the accelerator

Figure 14 demonstrates the thrustor performance with the internal countercurrent stream of electrons The left side of Fig 14 shows typical beam profiles with no backstreaming The right-side profiles show the effect obtained with the internal electron emitter operating Figure 15a shows the corresponding total power measurements computed from the profiles There is no doubt that the electron emitter greatly increases the ion beam power However, it is uncertain whether the increase in power brought about the emitter is due to the same mechanism that produced the local peaks observed in Fig 13 Unfortunately, the thrustor was operated with a very high neutral cesium flow rate for a portion of the data shown in Fig 15a The excess cesium probably caused the high accelerator impingement currents which were observed in these tests It remains to be shown in future research whether the excess neutrals play any role in the observed phenomena Figure 15b shows the three highest current points obtained with the internal electron emitter-accelerator system The highest point corresponds to an increase of 25 times over that of Child's law

It is impossible to prove that the increased power is due to ions only from the data at hand However, it does not seem reasonable that the vaporizer limited values of power would follow the normal curve (Fig 15a) if high-energy electrons were causing the great increase in power It would appear that if high-energy electrons were causing the observed increase in calorimeter power they would be unaffected by vaporizer temperature

The present accelerator configuration represents a first attempt to augment the Pierce accelerator system It appears to have led to much larger gains in ion current than electrical space-charge limitation will allow The present augmented accelerator results in no way represent the maximum power that even the present ion rocket might be made to produce Thus, large gains in total power might be obtained with a modified thrustor using counter-current electron flows to avoid space-charge limitations

Concluding Remarks

The physics of contact surface ionization of cesium on porous tungsten and rectilinear space-charge flow are well understood from the viewpoint of engineering design of ion thrustors The experimental research reported here supports this statement A gas flow calibration of the ionizer enabled the cesium flow rate through the tungsten emitter to be calibrated accurately for vapor pressure control Reynold's analysis[10] predicted the observed critical ion emission temperatures reasonably well The simple analytic solution of Pierce for space-charge limited ion accelerarors predicted the thrustor performance as a first approximation. However, the effect of the exit accelerator aperture is significant Deviations from Child's law were -34% at an accelerator aspect ratio L/D of 0 60 and diminished to -22% at $L/D = 1\ 3$ Of course, a more complete design analysis of aperture effects could be made using electrolytic tank analogs to bring analysis in line with experiment However, two unexpected phenomena occurred which are important to thrustor performance and which remain essentially unexplained The ratio of accelerator impingement currents to ion beam current showed a distinct minimum when space-charge limited operation was reached, and at slightly less than saturation current the accelerator operation was very unstable Similar independent observations were reported in some later research [16] Finally, local peaks in ion beam power were observed when high accelerator impingement currents occurred This increase in beam power may be due to backstreaming secondary electrons, and subsequent research tended to support this contention The use of backstreaming electron currents in electrostatic ion accelerators may offer a means of increasing beam power above Child's law predictions Research on some basic aspects of ion accelerators with countercurrent electron flow is now underway at Colorado State University sponsored by a NASA research grant of the Electric Propulsion Office, Cleveland, Ohio

References

[1] Stuhlinger, E , "Possibilities of electrical space ship propulsion," *Proceedings Fifth International Astronautics Congress* (Springer-Verlag, Vienna, 1955), pp 100–119

[2] Mickelsen, W R , "Comparative performance of electrostatic rocket engines," IAS Paper 62 74 (January 1962)

[3] Baldwin, L V and Sandborn, V A , "Theory and application of hot-wire calorimeter for measurement of ion beam power,' *Progress in Astronautics and Rocketry: Electrostatic Propulsion* edited by D B Langmuir, E Stuhlinger, and J M Sellen Jr (Academic Press Inc , New York, 1961), Vol 5, pp 425–446

[4] Baldwin, L V and Sandborn, V A , "Hot-wire calorimetry: theory and application to ion rocket research," NASA TR R-98 (1961)

[5] Keller, T A , "NASA electric rocket test facilities," National Vacuum Symposium, Cleveland, Ohio, Paper R25 (October 1960)

[6] Daykin, P N , "Electrode shapes for a cylindrical electron beam," Brit J Appl Phys **6**, 248–250 (1955)

[7] Pierce, J R , *Theory and Design of Electron Beams*, (D Van Nostrand Co , Inc , New York, 1954), 2nd ed, pp 181–182

[8] Lockwood, D L , Mickelsen, W R , and Hamza, V , "Analytic space charge flow and theoretical electrostatic rocket engine," ARS Paper 2400-62 (March 1962)

[9] Richley, E A , Sandborn, V A , Baldwin, L V , and Dangle, E E , "Comparative measurements of beam power in ion rocket research," NASA TN D-845 (May 1961)

[10] Reynolds, T W and Kreps, L W , "Gas flow, emittance, and ion current capabilities of porous tungsten," NASA TN D-871 (1961)

[11] Honig, R E , "Pressure data for the more common ele ments," Radio Corporation of America Review **XVIII,** 195–204 (June 1957)

[12] Taylor, J B and Langmuir, I , "The evaporation of atoms ions, and electrons from caesium films on tungsten," Phys Rev **44,** 423–458 (September 1933)

[13] Reynolds, T W and Childs, J H , "A graphical method for estimating ion-rocket performance, ' NASA TN D-466 (1960)

[14] Kuskevics, G , Marchant, A G , and Forrester, A T , "Surface ionization microscope," AIAA Paper 63016 (March 1963)

[15] Richley, E A and Mickelsen, W R , "Effects of molecular flow in plasma generation and some analyses of space charge flow in ion acceleration," AIAA Paper 64-7 (January 1964); also NASA Lewis TP 21-63 (1963)

[16] Wasserbauer, J F , "Experimental performance of a high current density cylindrical concave porous tungsten emitter for ion engines," AIAA Paper 63029 (April 1963)